Myotis bat STING attenuates aging-related inflammation in female mice

Xi Wang[1,2,3,#], Jing-Kun Jia[1,2,3,#], Qi Wang[1,2,3,#], Jing-wen Gong[1,2], Ang Li[2,4], Jia Su[1,2,3], Peng Zhou[1,2,4,*]

Affiliations:

1. Wuhan Institute of Virology, Chinese Academy of Sciences, Wuhan, Hubei 430071, China
2. Guangzhou National Laboratory, No.9 XingDaoHuanBei Road, Guangzhou International Bio Island, Guangzhou, Guangdong Province 510005, China
3. University of Chinese Academy of Sciences, Beijing 100000, China
4. State Key Laboratory of Respiratory Disease, The First Affiliated Hospital of Guangzhou Medical School, Guangzhou, Guangdong Province 510005, China

[#]These authors contributed equally.

[*]Correspondence: zhou_peng@gzlab.ac.cn (P.Z.)

ABSTRACT

As the only flying mammal, bats serve as natural reservoir hosts for numerous highly pathogenic viruses in humans (e.g., SARS-CoV or Ebolavirus). Furthermore, bats boast an unparalleled longevity among mammals relative to their size, particularly the *Myotis* bats that can live up to 40 years. However, the mechanisms underlying these distinctive traits remain incompletely understood. In our prior research, we demonstrated that bats exhibit dampened STING-interferon activation, potentially conferring upon them the capacity to mitigate virus- or aging-induced inflammation. To substantiate this hypothesis, we established the inaugural in vivo bat-mice model for aging studies by integrating *Myotis davidii* bat STING (*Md*STING) into the mice genome. We monitored genotypes and conducted a longitudinal comparative transcriptomics analysis on *Md*STING and wildtype mice over a 3-year aging process. Our plasma transcriptomics analysis indicated a reduction in aging-related inflammation in female *Md*STING mice, and the finding was further corroborated by in vivo data, demonstrating significantly lower levels of pro-inflammatory cytokines or chemokines, immunopathology, and neutrophil recruitment in aged female *Md*STING mice compared to aged wild-type mice. These results showed that *Md*STING knock-in attenuates aging-related inflammatory response and may also improve the healthspan in mice in a sex-dependent manner. Although the mechanism behind awaits further study, this work holds critical implications for bat longevity research, contributing to our comprehension of healthy aging in humans.

Keywords: Bat; STING; Longevity; Aging-related inflammation; Virus reservoir host

INTRODUCTION

Being the only mammals capable of powered flight, bats exhibit a multitude of distinctive biological traits (Dejosez et al., 2023; Irving et al., 2021; Teeling et al., 2018). On one hand, bats are recognized as natural reservoir hosts for numerous highly pathogenic viruses, some of which have precipitated large-scale infectious diseases in humans, such as SARS-related coronaviruses and Ebolavirus (Dejosez et al., 2023; Irving et al., 2021; Ruiz-Aravena et al., 2022; Teeling et al., 2018). On the other hand, bats boast an unparalleled longevity among mammals relative to their size (Austad, 2009; Brunet-Rossinni and Austad, 2004; Power et al., 2022). For instance, the bat genus with the greatest longevity, Myotis, can live up to 40 years (Healy et al., 2014). However, the mechanisms underlying these unique characteristics, particularly in their roles as viral reservoir hosts and long-lived animals, remain inadequately understood.

In recent years, research efforts have predominantly centered on unraveling the distinctive coexistence between bats and viruses (Dejosez et al., 2023; Irving et al., 2021; Ruiz-Aravena et al., 2022; Teeling et al., 2018). Our work, along with others', has demonstrated that bats possess a constitutively expressed interferon system while concurrently exhibiting a dampened stimulator of interferon genes (STING) and inflammatory responses (Ahn et al., 2019; Fu et al., 2023; Xie et al., 2018; Zhou et al., 2016). This characteristic may confer an early inhibition of viral replication or a moderated immune response upon viral infection. It is noteworthy that a low-level, over-dosed inflammatory response is also a hallmark of human aging, attributed to the

senescence-associated secretory phenotype (SASP), primarily dependent on the DNA-cGAS-STING pathway (Gulen et al., 2023; Pan et al., 2023; Victorelli et al., 2023; Zhang et al., 2022; Zhao et al., 2023). Therefore, it is conceivable that the dampened STING/NLRP3 inflammatory responses observed in bats may contribute to the mitigation of aging-related inflammation, thus promoting an extended healthspan in bats (Ahn et al., 2019; Xie et al., 2018). In a longitudinal comparative transcriptomics analysis, it was revealed that bats exhibit a unique, age-related gene expression pattern associated with DNA repair, autophagy, immunity, and tumor suppression (Huang et al., 2019). These findings suggest that these factors may be instrumental in driving the prolonged healthspan observed in bats (Huang et al., 2019). However, it is important to note that these observations are primarily observational and lack in vivo confirmation. Remarkably, until the recent bat ASC2-mice study conducted last year, there has been a scarcity of in vivo investigations into bat functional genes due to the current limitations in gene modulation in bats(Ahn et al., 2023). A most recently published study showing that a transgenic mouse overexpressing naked mole-rat hyaluronic acid synthase 2 gene has prolonged healthspan (Zhang et al., 2023), which has set a good paradigm for characterizing unique genes related to lifespan and healthspan in model organisms.

We previously identified the universal replacement of the serine 358 residue (one of the critical activation residues) in STING in bats, resulting in the dampening of downstream interferon responses and antiviral activity (Xie et al., 2018). In recent years, extensive research has delved into the role of STING in the human aging

process (Huang et al., 2023; Pan et al., 2023; Paul et al., 2021). It has been demonstrated that the cGAS–STING pathway acts as a driver of the senescence-associated secretory phenotype (SASP) in humans, and blocking cGAS–STING signaling emerges as a potential strategy to impede neurodegenerative processes in old age (Gulen et al., 2023; Zhang et al., 2022; Zhao et al., 2023). Consequently, we hypothesized that bat STING, with its unique dampened character, may contribute to the relatively extended healthspan observed in bats. In this study, we created a *Myotis davidii* bat STING (*Md*STING)-knock-in mouse model and conducted a comprehensive comparison of aging-related genotypes with wild-type mice over a 3-year period. To our knowledge, this represents the inaugural animal model in the field of bat aging, paving the way for unraveling the mechanisms underpinning the exceptional longevity observed in bats.

MATERIALS AND METHODS

Establishment of Myotis STING mouse model

C57BL/6J wild-type (WT) mice were purchased from Beijing Vital River Laboratory Animal Technology Co., Ltd. The designing, establishment and validation of *Md*STING mice was conducted by the authors and Shanghai Biomodel Organism Science & Technology Development Co., Ltd (Figure 1; Supplementary Figure S1). Briefly, *M.d* STING$^{+/+}$ (*Md*STING) mice utilized in this study were generated through micro-injection of a donor vector, in vivo-transcribed Cas9 mRNA, and gRNA (GTGACCTCTGGGCCGTGGGA) into fertilized ovum (C57BL/6J background). The donor vector contains 5'/3' homologous arms and *M.d* STING-WPRE-poly A

106 sequences. The *M.d* STING-WPRE-poly A sequences were precisely inserted
107 downstream of the ATG start codon in the third exon of the mouse STING gene,
108 guarantee the accurate transcriptional expression of the bat STING gene.
109 Simultaneously, the mouse STING gene was disrupted through targeted knockout
110 during the knock-in procedure.
111 All animal experiments conducted in this study received approval from the Ethics
112 Committee of the Wuhan Institute of Virology, Chinese Academy of Sciences, under
113 approval number WIVA43202105. The experiments were conducted according to the
114 fundamental guidelines for the welfare of experimental animals.
115
116 **Cell culture and transfection**
117 293T cells were cultured in Dulbecco's modified Eagle medium (DMEM) (Gibco,
118 USA) supplemented with 10% (v/v) fetal bovine serum (FBS) (Gibco, USA) under
119 5% CO_2 at 37°C. *Myotis davidii*, *Homo sapiens*, and *Mus musculus* STING genes
120 were cloned into the pCAGGS vector with a C-terminal S-tag. Before transfection, the
121 correctness of STING plasmids was confirmed by sequencing. Transfections were
122 conducted using Lipofectamine 3000 (Thermo, USA) according to the manufacturer's
123 protocol. Primary mouse bone marrow cells were harvested and differentiated into
124 bone marrow-derived macrophages (BMDMs) over a 6-day period using RPMI 1640
125 supplemented with 10% (v/v) FBS and 20 ng/mL macrophage colony-stimulating
126 factor (M-CSF) (Peprotech, USA) under 5% CO_2 at 37°C. Splenocytes were obtained
127 by pressing spleen tissues through a cell strainer using a disposable abrasive stick.

The collected splenocytes were then treated with 1× RBC lysis buffer (eBioscience, USA). Subsequently, the splenocytes were washed twice with PBS and resuspended in RPMI 1640 supplemented with 10% (v/v) FBS.

Mice genotype determination

Genotype determination was performed at 2 weeks of age. Toes were excised and lysed in 300 μL of 50 mmol/L NaOH at 95°C for 30 minutes. Subsequently, 25 μL of 1 mol/L Tris-HCl (pH 8.0) was added and thoroughly mixed. Following treatment, the lysed samples were utilized as templates for PCR-based genotype determination. The primers used were as follow: Primer F :5'- GGGGCTCACATGTACACGCTCTG-3'; Primer R: 5'- CGCGCACAGCCTTCCAGTAG-3'.

Lifespan study and sample collection

WT/*M.d* STING$^{+/+}$ mice utilized in this study were individually housed by gender and maintained in the animal facility of the Wuhan Institute of Virology, Chinese Academy of Sciences. Each cage accommodated six mice, with a 12-hour light/dark cycle and a room temperature of 25°C. The lifespan was counted to WT/*M.d* STING$^{+/+}$ mice cohorts (n=6 male or female for STING mice, n=5 male/9 female for WT mice), started from 3 months age until their death. Moreover, blood samples were also collected from each of these mice for every 3 months using EDTA·2Na (BBI, CN) as an anticoagulant. In total, plasma samples were collected at 3 (n=26), 6 (n=26), 9 (n=26), 12 (n=26), 15 (n=23), 18 (n=21), 24 (n=13) and 29 (n=3) months

for each mouse. Weight and mortality were recorded prior to each blood collection. Mice surviving until the 29th month were anesthetized and euthanized at that juncture. For pathological confirmation of the plasma transcriptome data, female mice at 1.5 months and 13 months of age were selected (n=4). These mice were anesthetized with Avertin, blood samples were collected from the eyeballs, and subsequently, the mice were euthanized. Tissue samples from the heart, liver, spleen, lung, kidney, intestine, brain, and muscle were collected and partitioned into multiple portions. Tissues designated for qRT-PCR analysis were directly preserved in tubes containing VeZol Reagent (R411-02, Vazyme, CN) along with beads for tissue homogenization. Tissues intended for hematoxylin and eosin (HE) staining and Immunohistochemistry (IHC) were fixed in 4% paraformaldehyde (PFA) (BL539A, Biosharp, CN). Blood samples were fractionated for RNA extraction and ELISA testing.

RNA extraction and RNA sequencing

Total RNA from blood samples was lysed using VeZol Reagent (R411-02, Vazyme, CN), and subsequent total RNA extraction was performed following the manufacturer's instructions. Tissue samples in VeZol were initially homogenized using the Tissue Cell-destroyer 1000 (NZK, CN) at recommended settings, followed by total RNA extraction as per the provided manual.

RNA samples obtained from mouse blood were submitted to BGI (Beijing, CN) for sequencing. The RNA sequencing (RNA-seq) library construction and subsequent

sequencing procedures were conducted at BGI. The filtered sequencing data were processed using a standard pipeline. In Linux, raw reads were aligned to the respective homologous genomes using Hisat2 (v2.1.0) (Kim et al., 2019)and Samtools (v1.17) (Danecek et al., 2021). For data originating from wild-type mice, the mouse genome (GCF_000001635.27) (https://www.ncbi.nlm.nih.gov/datasets/genome/GCF_000001635.27/) was employed as a reference, whereas the edited genome was utilized for data derived from *Md*STING mice. Subsequently, StringTie (v2.2.1) (Shumate et al., 2022)was employed for transcript assembly and qualification, utilizing high-quality genome annotation. Samples exhibiting an overall alignment rate exceeding 80% were selected for subsequent analyses. Genes expressed across all samples were subjected to differential expression analysis in the R program (v4.3.1) (https://www.r-project.org/). Samples were categorized based on age and gender. Transcriptomic alterations in gene expression were compared between *Md*STING mice and wild-type mice. DESeq2 (v1.40.2) (Love et al., 2014) was utilized for differential gene expression analysis, with all parameters set to default values. The quality of raw reads was assessed using FastQC (v0.11.9) (https://www.bioinformatics.babraham.ac.uk/projects/fastqc/). The counts matrix was analyzed using R (v4.2.1) (https://www.r-project.org/). The R package DESeq2 (v1.36.0) was employed for normalization and identification of differentially expressed genes (DEGs) (Love et al., 2014). Gene Set Enrichment Analysis (GSEA) was conducted using the R package clusterProfiler v(4.4.4) (Wu et al., 2021). The

fraction of neutrophils and monocytes/macrophages was inferred using ImmuCellAI-mouse (v0.1.0) (Miao et al., 2022). Statistical analyses were performed using Stats (v4.2.1) (https://search.r-project.org/R/refmans/stats/html/00Index.html). Data visualization was achieved using pheatmap (v1.0.12) (https://cran.r-project.org/web/packages/pheatmap/index.html)and ggplot2 (v3.3.6) (Wickham, 2016).

Quantitative real-time PCR (qRT-PCR)

qRT-PCR experiments were conducted using the CFX Duet Real-Time PCR system (Bio-Rad, USA). PCR settings and mix preparation were based on the instructions provided by the HiScript II One Step qRT-PCR SYBR Green Kit (Q221, Vazyme, CN). Specific primer pairs were employed to assess mRNA levels of the corresponding genes (Supplementary Table S1).

Western blot

293T or BMDM cells were lysed using Western and IP lysis buffer (Beyotime, CN) supplemented with protease and phosphatase cocktail inhibitors (Thermo Fisher) for 15 minutes. The lysates were then mixed with 6× SDS loading buffer and boiled at 95°C for 10 minutes. Equal amounts of protein were loaded onto SDS-PAGE gels, followed by transfer onto a 0.22 μm PVDF membrane. The membrane was subsequently blocked with rapid blocking solution for 10 minutes. Primary antibodies (anti-S-tag, 1:3 000, Abcam, UK; anti-GAPDH, 1:5 000, Proteintech, CN; anti-

STING, 1:1 000, CST, GER) were then incubated overnight, followed by washing with TBS containing 0.1% Tween for 30 minutes. The membrane was then incubated with secondary antibodies (HRP-conjugated anti-mouse/rabbit IgG, 1:10 000, Proteintech, CN) at room temperature for 1 hour, followed by another 30-minute wash. Finally, the membrane was exposed to an ECL chemiluminescent substrate (Vazyme, CN) using a ChemiDoc XRS$^+$ (Bio-Rad, USA) imaging system.

ELISA

Plasma samples from female mice aged 1.5 months and 13 months were collected, with 4 mice per group. The concentration of IL-1β in the plasma was quantified using the mouse IL-1β ELISA kit (CME0015, 4ABio, CN) according to the manufacturer's instructions.

HE and Immunohistochemistry

The livers of female mice aged 1.5 months and 13 months were collected (n=4 in each group). Fresh tissues were fixed in 4% paraformaldehyde for over 24 hours, subsequently embedded in paraffin, and then sectioned into 4μm thick slices for histological or immunohistochemical (IHC) analyses. For histological assessment, these sections were stained with hematoxylin (Servicebio, CN) to visualize the nuclei and eosin (Servicebio, CN) to delineate the cytoplasm. This staining facilitated the observation of the tissue's normal morphology as well as the infiltration of immune cells. For IHC, these sections were incubated with anti-mouse Ly6G primary antibody

(GB11229, 1:300, rabbit, Servicebio, CN). Subsequently, the sections were stained with fluorescently labeled secondary antibodies (anti-rabbit FITC, GB22403, 1:200, Servicebio, CN) and DAPI (G1012, Servicebio, CN) for nuclear staining. Fiji Image J (NIH) software was utilized for the analysis of inflammatory cell area and positive cell counts in IHC staining.

Statistical analysis

Data are presented as mean ± standard error of the mean (s.e.m.), unless stated otherwise. 'n' denotes the number of animals per test group, with age and sex also noted. Randomly selected littermates were utilized for all experiments. Statistical analyses were conducted using GraphPad Prism 8.4.3 (GraphPad, USA). *P* values were derived from a two-tailed unpaired t-test. Lifespan data were analyzed using Kaplan–Meier survival curves, with *P* values calculated via log-rank test. All relevant *P* values are depicted in the figures.

RESULTS

Establishment of Myotis bat STING knock-in mice

To elucidate the role of STING in the extended healthspan observed in bats, we engineered knock-in mice harboring the *Myotis davidii* STING gene (*Md*STING), which had demonstrated notable dampening of interferon activation in response to viral or cGAMP stimulation in our previous study (Xie et al., 2018). Employing CRISPR-Cas9 technology (Ma et al., 2018), we introduced the *Myotis davidii* STING

gene into exon 3 of the mouse STING gene in wild-type C57BL/6J mice (Figure 1A; Supplementary Figure S1). Homozygous *M.d* STING$^{+/+}$ mice were generated through heterozygous breeding, and the correct insertion of *M.d* STING gene was confirmed via genomic DNA sequencing or PCR analysis (Figure 1B; Supplementary Figure S1A; Supplementary Data S1). We also observed the expression of STING protein in mice, and the results indicated that the size was same to that of exogenously transfected STING protein (Figure 1C). Notably, the molecular weight of *M.d* STING is higher than that of human or mice STING naturally, probably due to the difference in posttranslational modifications such as glycosylation, as *M.d* STING contains more O-glycosylation sites compared to that of mice and humans (Supplementary Figure S1B). The expression pattern of the *Md*STING gene in different mouse organs was also verified, revealing no discernible differences compared to wild-type mice (Figure 1D). Finally, to validate the functionality of bat STING, we stimulated splenocytes from wild-type and bat STING knock-in mice with cGAMP. The data revealed that bat STING KI mice manifested a dampened type I interferon response (Figure 1E), consistent with our previous study (Xie et al., 2018). Collectively, the Myotis *STING* gene was successfully inserted into the mice genome with correct size, maintaining a comparable expression pattern and dampened IFN activation (same as exogenously transfected Myotis STING protein) compared to wild-type mice.

Longitudinal comparative transcriptomics analysis reveals reduced aging-related

inflammation responses in bat STING-KI mice

To explore whether *Md*STING may attenuate ageing-related inflammation and further improve the healthspan in mice, we conducted a longitudinal comparative study involving both wild-type and *Md*STING mice. The cohort, comprising an equal number of male and female mice, underwent continuous monitoring of lifespan and body weight. Additionally, blood samples were collected from each mouse every 3 months via retro-orbital bleeding, spanning intervals of 0, 3, 6, 9, 12, 15, 18, 24 and 29 months of age, for subsequent transcriptome analysis (Figure 2A). In total, the monitoring extended for over 3 years, encompassing a period of 37 month. Our data reveal that wild-type and bat STING KI mice maintain similar body weights throughout their lifespan (Supplementary Figure S2). Albeit showing no statistical significance, the female *Md*STING mice appear an extended median lifespan compared to control mice, whereas the trend was not observed in male mice (Supplementary Figure S2). It should be noted that this observation of prolonged lifespan was based on the relatively small cohort size and more animals of both genders should be monitored in the future.

Given the possible extended median lifespan observed in female *Md*STING mice, we proceeded to investigate whether this gene contributed to an overall improvement in health status. Through a longitudinal comparative transcriptomics analysis of mouse blood during the aging process, we identified a consistent pattern of up- or down-regulation of genes in aged mice (after 12 months) compared to their younger

303 counterparts. Notably, female *Md*STING mice exhibited a discernible alleviation in
304 aging-related genes and pathways when compared to wild-type female mice (Figure
305 2). These findings were not observed in the blood transcriptome analysis of male mice
306 (Supplementary Figure S4). This observation suggests that the introduction of
307 *Md*STING has a potential role in mitigating aging-related inflammation responses,
308 contributing to the overall enhanced health status in these mice.

309 To discern the molecular pathways underlying the observed differences between aged
310 *Md*STING and wild-type mice, we initiated Gene Set Enrichment Analysis (GSEA)
311 (Subramanian et al., 2005) on differentially expressed genes. Notably, pathways
312 associated with neutrophil and TNF activation exhibited time-dependent lower
313 expression in the aged *Md*STING mice (Figure 2B), indicating a potential role in
314 STING-dependent aging-related inflammation (Victorelli et al., 2023). Enrichment of
315 epidermal cell differentiation, likely attributed to regular retro-orbital bleeding
316 damage, was also identified. Further exploration encompassed 4864 pathways
317 displaying consistent differences across all time points. Pathways linked to neutrophil
318 activation, degranulation, and leukocyte inflammatory response were significantly
319 down-regulated in aged *Md*STING mice compared to wild-type mice (Figure 2C, D).
320 Conversely, pathways associated with the cell cycle demonstrated significant
321 upregulation in aged *Md*STING mice (Figure 2E). Given that cell cycle arrest is a
322 hallmark of aging (Cai et al., 2022), our data suggests that aged *Md*STING mice
323 exhibit blood transcriptome characteristics akin to younger mice.

To further elucidate the consequences of differential genes and pathways, we assessed the inferred proportions of neutrophils, monocytes, and macrophages in both wild-type and *Md*STING mice at each time point (Figure 2F, G). Our findings indicate that *Md*STING mice exhibited lower overall levels of inflammatory myeloid cells, including neutrophils, monocytes, and macrophages, compared to wild-type mice (Figure 2F, G). Finally, we examined the expression differences of a panel of inflammation-related genes in blood transcripts between aged *Md*STING and wild-type mice. Notably, the expression of genes such as *Lcn2* (neutrophil cytokine signaling), *Ngp* (neutrophilic granule protein), *Cxcr2* (neutrophil, mononuclear macrophage chemokine receptor), *Ifngr1* (interferon gamma receptor), *Nlfam1* (monocyte pro-inflammatory responses), *Tnfaip3* (ameliorates the degeneration of inflammatory response), *Il1b* (major inflammatory cytokine), *Il7r* (T cell activation-related receptor), and *Il17ra* (Il17 receptor, related to Th17 response) were significantly lower in aged *Md*STING female mice at least at one time point during the aging process (Supplementary Figure S3), but not in aged male mice (Supplementary Figure S4). Collectively, our data suggested that *Md*STING mice exhibit alleviated aging-related inflammation in female mice.

Bat STING reduces pro-inflammatory cytokines and chemokines in vivo

Our data suggest that *Md*STING mice improves the profiles of aging-associated secretory cytokines (SASP) in mice blood during the aging process. To validate these

findings in vivo, we selected two groups of young (1.5 months) and aged (13 months) mice for both wild-type and *Md*STING mice for further comparison. The 13-month group was specifically chosen, as it exhibited the most substantial difference in healthspan in our previous results. Subsequently, we dissected the mice and compared the expression of a panel of SASP cytokines and the recruitment of pro-inflammatory white blood cells (WBCs) in various mouse organs (Figure 3; Figure 4; Supplementary Figure S5).

Given the marked downregulation of the TNF pathway in *Md*STING female mice, we initially measured the *Tnf-a* mRNA expression in aged female mice and the serum cytokines for the different mouse groups. Consistent with our gene expression data, both *Tnf-a* and IL-1β proteins were upregulated during the aging process in wild-type female mice but not in *Md*STING female mice (Figure 3A, B). Subsequently, we assessed a panel of SASP-related cytokines and chemokines in various organs, including the liver, kidney, heart, spleen, intestine, lung, blood, and muscle. As observed in previous aging-related mouse models (Zhang et al., 2023), the liver and kidney exhibited the most significant phenotype differences (Figure 3C, D; Supplementary Figure S5). In comparison to young mice, aged wild-type mice displayed a substantial increase in SASP-related cytokines (*Tnf*, *Il1b*, *Il17* in the liver and *Tnf*, *Il1b*, *Il6* in the kidney) and SASP-related chemokines (*Cxcl9*, *Cxcl10*, *Ccl2* in the liver and *Cxcl10*, *Ccl2*, *Mmp12* in the kidney). Conversely, the majority of these genes either exhibited lower expression or showed no age-dependent upregulation in *Md*STING mice. Additionally, one or more SASP-related genes

(Birch and Gil, 2020) were upregulated in aged wild-type mice but not in *Md*STING mice in other organs (Supplementary Figure S5A-F). These findings collectively suggest that aging leads to increased expression of inflammatory genes, and STING plays a regulatory role during the aging process, with the dampened *Md*STING resulting in reduced aging-related proinflammatory cytokines.

Bat STING reduces the aging-related immunopathology in mice

Subsequently, we assessed physiological changes during the aging process, specifically conducting immunopathology analysis on the liver, a site showing significant SASP-related cytokine differences between wild-type and *Md*STING mice. The liver is susceptible to degenerative changes such as increased inflammation and fibrosis, diminished regenerative capacity, and reduced repair ability after injury, leading to the development of related diseases during aging (Hoare et al., 2010; Zhang et al., 2023). We choose 13-month mice for comparison between STING mice and wild type mice, as mice start to show aging-related inflammation at the time point. In our data, mild fatty lesions were observed in the aged livers (13 months) for all groups. Notably, we observed significant foci of inflammatory cell infiltration in the aged wild-type mice but not in *Md*STING mice, particularly in the Kupffer cells (Figure 4A, B). This observation suggests that *Md*STING mice exhibit reduced aging-related immunopathology compared to their wild-type counterparts.

Additionally, we observed a significant influx of neutrophils exclusively in aged wild-type mice (Figure 4C, D), aligning with our prior observation of low neutrophil activation in *Md*STING mice. To further pinpoint indicators of liver neutrophil activation, we examined the expression of immune cell markers and cytokine receptors through qRT-PCR. The qPCR data revealed a notably higher expression of *Cd11b* myeloid cell markers, neutrophil activation-related indicators such as the *Mpo* gene, *Cxcr2*, and *Cxcr4* in aged wild-type mice compared to *Md*STING mice (Figure 4E). These findings, coupled with limited pathological changes, reduced immune cell recruitment, and mitigated inflammation during aging in *Md*STING mice, underscore the crucial role of bat STING in enhancing healthspan in mice.

DISCUSSION

To our knowledge, this study represents the first in vivo exploration elucidating potential mechanisms underlying the exceptional longevity observed in bats. Through the utilization of a knock-in mouse model, we show that Myotis bat STING attenuated aging-related pro-inflammatory cytokines/chemokines and curtailing the recruitment of pro-inflammatory immune cells, although in a gender-dependent manner in mice. This conclusion is supported by both longitudinal comparative transcriptomics analysis and subsequent experimental validation. Building upon our previous identification of a dampened STING-interferon response (Xie et al., 2018), our findings suggest that STING may play a role in the extended lifespan of bats.

In human, aging has been a risk factor for many chronic diseases, for example cancer

(Cai et al., 2022).Beyond the scope of aging-related research in humans, there has been a growing interest in studying longevity animals to unravel potential anti-aging mechanisms (Stenvinkel and Shiels, 2019; Tian et al., 2017; Zhao et al., 2021). Two mammals that have garnered attention in recent years are the naked-mole rat and bats, both exhibiting extended lifespans compared to mammals of similar size (Baid et al., 2024; Gorbunova et al., 2020; Huang et al., 2019; Oka et al., 2023; Zhang et al., 2023). However, a significant challenge in studying these animals lies in the lack of in vivo animal models and related reagents. Recent publications have demonstrated that overexpressing high molar mass hyaluronic acid (HMM-HA) from the naked-mole rat successfully increased healthspan in mice, providing valuable insights through the use of transgenic mice as a tool for studying non-model animals (Zhang et al., 2023). Similarly, while there have been studies suggesting that bats may possess unique aging-related pathways, the absence of in vivo data has limited the validation of these conclusions (Huang et al., 2019; Irving et al., 2021; Li et al., 2023). In this context, our data holds important implications, showing that bat genes can mitigate aging-related inflammatory responses offers potential for extending the healthspan of mice. This highlights the utility of genetically modified mice as an in vivo model for investigating bat anti-aging mechanisms. The success of this model paves the way for the exploration of more bat genes, such as those involved in DNA damage repair (e.g., P53, ATM, and SETX) (Zhao et al., 2023), which have been positively selected and are believed to play a role in the longevity of bats (Zhang et al., 2013).

Our study demonstrated that dampened STING functionality contributes to anti-aging effects. In the human aging process, senescence and the senescence-associated secretory phenotype (SASP) are pivotal, heavily reliant on the cGAS-STING pathway, which recognizes fragmented nuclear or mitochondrial DNA (Gulen et al., 2023; Hu and Shu, 2023; Victorelli et al., 2023). These aging-related danger signals contribute to a low-level pro-inflammatory state, eventually leading to chronic organ aging (Cai et al., 2022). Consequently, STING has emerged as an intriguing target for interventions aimed at addressing aging-related diseases (Huang et al., 2023; Pan et al., 2023; Zhang et al., 2022; Zhao et al., 2023). A previous study showing that blockade of STING using a small molecule H-151 suppresses the inflammatory phenotypes of senescent human cells and tissues, attenuates ageing-related inflammation in multiple peripheral organs and the brain in mice (Gulen et al., 2023). In comparison, bat STING, while naturally dampened, retains functionality(Xie et al., 2018). Our data demonstrate a similar effect, with reduced cytokine release and immune cell recruitment akin to the effects observed with H-151 or HMM-HA in mice (Gulen et al., 2023; Zhang et al., 2023). This suggests that bat STING could be a promising target for anti-aging studies, offering potential avenues for further research and therapeutic development.

There are several limitations in our study, and improvements can be considered in future research. Firstly, although the in vitro data show an attenuated aging-related inflammation in Myotis STING KI mice, we failed to observe a significant improvement of healthspan in mice. Moreover, investigating aging-related

452 immunopathology separately in male and female Myotis STING KI mice should be
453 performed to further demonstrate the sex biased effect on aging (Xiao et al., 2024),
454 especially in context of our finding that attenuated aging-related inflammation in
455 *Md*STING female mice. This discrepancy could be attributed to the relatively smaller
456 cohort size of mice compared to other aging cohorts, and the number of mice used
457 was simply insufficient for a lifespan study. Thus, the findings of our current study
458 should be considered preliminary results. We would need a legitimate aging study
459 with the appropriate number of animals to derive legitimate aging results in future
460 work. Secondly, while our data propose a significant functionality of STING in bats,
461 the exact mechanism regarding how STING dampened aging-related inflammation in
462 our model remains to be elucidated. The dampened interferon and inflammation
463 pathways by bat STING protein may play a role, but there is a possibility for other
464 signaling pathways to be involved in this process, especially when we considered the
465 fact that aging is a very complex process (Benayoun et al., 2015; Lopez-Otin et al.,
466 2023; Zhao et al., 2023). It remains imperative to validate bat STING indeed plays a
467 role using a bat model. Given the challenges associated with constructing bat
468 colonies, conducting cell senescence studies using bat pluripotent stem cells or bat
469 organoids (Dejosez et al., 2023) could be a viable alternative and will be considered in
470 future research. Thirdly, there is potential for the design of small molecules that
471 dampen, rather than completely block, the functionality of human STING (Pan et al.,
472 2023; Zou et al., 2023), mimicking the natural dampening observed in bats.
473 Additionally, exploring whether bat STING confers mice with resistance to viral-

induced inflammation would be interesting. This exploration may shed light on the unique coexistence between bats and viruses, providing valuable insights into the intricate relationship between the bat immune system and viral infections.

In summary, utilizing the in vivo model for studying bat anti-aging mechanisms, we have provided preliminary data to demonstrate that Myotis bat STING reduced aging-related pro-inflammatory responses and pathology, thus possibly improves the healthspan in mice. The findings underscore the potential of bat STING as a promising target for anti-aging studies and offer insights into mechanisms that may be harnessed for improving healthspan in mammals.

ACKNOWLEDGEMENTS

We appreciate the help of Fan Zhang, He Zhao, and Li Li from the animal center of Wuhan Institute of Virology. This work was jointly supported by the China Natural Science Foundation for outstanding scholars (82325032 to P.Z.) and the Self-Supporting Program of Guangzhou Laboratory (SRPG22-001 to P.Z.).

DATA AVAILABILITY

The raw RNA-seq data analyzed in this study are available from the NCBI database (BioProject PRJNA1098971), China National Center for Bioinformation database of Genome Sequence Archive (GSA) (PRJCA025190), and Science Data Bank database

(doi: 10.57760/sciencedb.j00139.00129).

SUPPLEMENTARY DATA

Supplementary data to this article can be found online.

COMPETING INTERESTS

The authors declare that they have no competing interests.

AUTHORS' CONTRIBUTIONS

Z.P. conceived the concept; W.X. and Z.P. designed the study, W.X. and J.J.K. performed the experiments; W.X. analyzed the most of data; W.Q. and J.J.K. analyzed the RNA-seq data; G.J.W. and L.A. raised mice; S.J. collected the RNA-seq data. Z.P. and W.X. wrote the manuscript; Z.P. and W.X. revised the manuscript. All authors read and approved the final version of the manuscript.

REFERENCES

Ahn M, Anderson DE, Zhang Q, et al. 2019. Dampened NLRP3-mediated inflammation in bats and implications for a special viral reservoir host. *Nature Microbiology*, **4**(5): 789-799.

Ahn M, Chen VC, Rozario P, et al. 2023. Bat ASC2 suppresses inflammasomes and ameliorates inflammatory diseases. *Cell*, **186**(10): 2144-2159 e2122.

Austad SN. 2009. Comparative biology of aging. *Journals Of Gerontology Series A-biological Sciences And Medical Sciences*, **64**(2): 199-201.

517 Baid K, Irving AT, Jouvenet N, et al. 2024. The translational potential of studying bat
518 immunity. *Trends in Immunology*, **45**(3): 188-197.
519 Benayoun BA, Pollina EA, Brunet A. 2015. Epigenetic regulation of ageing: linking
520 environmental inputs to genomic stability. *Nature Reviews Molecular Cell Biology*, **16**(10):
521 593-610.
522 Birch J & Gil J. 2020. Senescence and the SASP: many therapeutic avenues. *Genes &*
523 *Development*, **34**(23-24): 1565-1576.
524 Brunet-Rossinni AK & Austad SN. 2004. Ageing studies on bats: a review. *Biogerontology*,
525 **5**(4): 211-222.
526 Cai Y, Song W, Li J, et al. 2022. The landscape of aging. *Science China-Life Sciences*,
527 **65**(12): 2354-2454.
528 Danecek P, Bonfield JK, Liddle J, et al. 2021. Twelve years of SAMtools and BCFtools.
529 *Gigascience*, **10**(2).
530 Dejosez M, Marin A, Hughes GM, et al. 2023. Bat pluripotent stem cells reveal unusual
531 entanglement between host and viruses. *Cell*, **186**(5): 957-974 e928.
532 Fu F, Shao Q, Zhang J, et al. 2023. Bat STING drives IFN-beta production in anti-RNA virus
533 innate immune response. *Frontiers in Microbiology*, **14**: 1232314.
534 Gorbunova V, Seluanov A, Kennedy BK. 2020. The World Goes Bats: Living Longer and
535 Tolerating Viruses. *Cell Metabolism*, **32**(1): 31-43.
536 Gulen MF, Samson N, Keller A, et al. 2023. cGAS-STING drives ageing-related inflammation
537 and neurodegeneration. *Nature*, **620**(7973): 374-380.
538 Healy K, Guillerme T, Finlay S, et al. 2014. Ecology and mode-of-life explain lifespan variation

539 in birds and mammals. *Proc Biol Sci*, **281**(1784): 20140298.

540 Hoare M, Das T, Alexander G. 2010. Ageing, telomeres, senescence, and liver injury. *J*

541 *Hepatol*, **53**(5): 950-961.

542 Hu MM & Shu HB. 2023. Mitochondrial DNA-triggered innate immune response: mechanisms

543 and diseases. *Cellular & Molecular Immunology*, **20**(12): 1403-1412.

544 Huang Y, Liu B, Sinha SC, et al. 2023. Mechanism and therapeutic potential of targeting

545 cGAS-STING signaling in neurological disorders. *Molecular Neurodegeneration*, **18**(1): 79.

546 Huang Z, Whelan CV, Foley NM, et al. 2019. Longitudinal comparative transcriptomics

547 reveals unique mechanisms underlying extended healthspan in bats. *Nature Ecology &*

548 *Evolution*, **3**(7): 1110-1120.

549 Irving AT, Ahn M, Goh G, et al. 2021. Lessons from the host defences of bats, a unique viral

550 reservoir. *Nature*, **589**(7842): 363-370.

551 Kim D, Paggi JM, Park C, et al. 2019. Graph-based genome alignment and genotyping with

552 HISAT2 and HISAT-genotype. *Nature Biotechnology*, **37**(8): 907-915.

553 Li KQ, Liu GJ, Liu XY, et al. 2023. EPAS1 prevents telomeric damage-induced senescence

554 by enhancing transcription of TRF1, TRF2, and RAD50. *Zoological Research*, **44**(3): 636-649.

555 Lopez-Otin C, Blasco MA, Partridge L, et al. 2023. Hallmarks of aging: An expanding

556 universe. *Cell*, **186**(2): 243-278.

557 Love MI, Huber W, Anders S. 2014. Moderated estimation of fold change and dispersion for

558 RNA-seq data with DESeq2. *Genome Biology*, **15**(12): 550.

559 Ma X, Wong AS, Tam HY, et al. 2018. In vivo genome editing thrives with diversified CRISPR

560 technologies. *Zoological Research*, **39**(2): 58-71.

Miao YR, Xia M, Luo M, et al. 2022. ImmuCellAI-mouse: a tool for comprehensive prediction of mouse immune cell abundance and immune microenvironment depiction. *Bioinformatics*, **38**(3): 785-791.

Oka K, Yamakawa M, Kawamura Y, et al. 2023. The Naked Mole-Rat as a Model for Healthy Aging. *Annual Review of Animal Biosciences*, **11**: 207-226.

Pan J, Fei CJ, Hu Y, et al. 2023. Current understanding of the cGAS-STING signaling pathway: Structure, regulatory mechanisms, and related diseases. *Zoological Research*, **44**(1): 183-218.

Paul BD, Snyder SH, Bohr VA. 2021. Signaling by cGAS-STING in Neurodegeneration, Neuroinflammation, and Aging. *Trends in Neurosciences*, **44**(2): 83-96.

Power ML, Foley NM, Jones G, et al. 2022. Taking flight: An ecological, evolutionary and genomic perspective on bat telomeres. *Molecular Ecology*, **31**(23): 6053-6068.

Ruiz-Aravena M, Mckee C, Gamble A, et al. 2022. Ecology, evolution and spillover of coronaviruses from bats. *Nature Reviews Microbiology*, **20**(5): 299-314.

Shumate A, Wong B, Pertea G, et al. 2022. Improved transcriptome assembly using a hybrid of long and short reads with StringTie. *PLoS Computational Biology*, **18**(6): e1009730.

Stenvinkel P & Shiels PG. 2019. Long-lived animals with negligible senescence: clues for ageing research. *Biochemical Society Transactions*, **47**(4): 1157-1164.

Subramanian A, Tamayo P, Mootha VK, et al. 2005. Gene set enrichment analysis: a knowledge-based approach for interpreting genome-wide expression profiles. *Proceedings of the National Academy of Sciences of the United States of America*, **102**(43): 15545-15550.

Teeling EC, Vernes SC, Davalos LM, et al. 2018. Bat Biology, Genomes, and the Bat1K

583 Project: To Generate Chromosome-Level Genomes for All Living Bat Species. *Annual Review*
584 *of Animal Biosciences*, **6**: 23-46.
585 Tian X, Seluanov A, Gorbunova V. 2017. Molecular Mechanisms Determining Lifespan in
586 Short- and Long-Lived Species. *Trends in Endocrinology and Metabolism*, **28**(10): 722-734.
587 Victorelli S, Salmonowicz H, Chapman J, et al. 2023. Apoptotic stress causes mtDNA release
588 during senescence and drives the SASP. *Nature*, **622**(7983): 627-636.
589 Wickham H. 2016. ggplot2: Elegant Graphics for Data Analysis. Springer International
590 Publishing.
591 Wu T, Hu E, Xu S, et al. 2021. clusterProfiler 4.0: A universal enrichment tool for interpreting
592 omics data. *The Innovation*, **2**(3): 100141.
593 Xiao T, Lee J, Gauntner TD, et al. 2024. Hallmarks of sex bias in immuno-oncology:
594 mechanisms and therapeutic implications. *Nature Reviews Cancer*.
595 Xie J, Li Y, Shen X, et al. 2018. Dampened STING-Dependent Interferon Activation in Bats.
596 *Cell Host & Microbe*, **23**(3): 297-301 e294.
597 Zhang G, Cowled C, Shi Z, et al. 2013. Comparative analysis of bat genomes provides insight
598 into the evolution of flight and immunity. *Science*, **339**(6118): 456-460.
599 Zhang Z, Tian X, Lu JY, et al. 2023. Increased hyaluronan by naked mole-rat Has2 improves
600 healthspan in mice. *Nature*, **621**(7977): 196-205.
601 Zhang Z, Zhou H, Ouyang X, et al. 2022. Multifaceted functions of STING in human health
602 and disease: from molecular mechanism to targeted strategy. *Signal Transduction and*
603 *Targeted Therapy*, **7**(1): 394.
604 Zhao Y, Seluanov A, Gorbunova V. 2021. Revelations About Aging and Disease from

605 Unconventional Vertebrate Model Organisms. *Annual Review of Genetics*, **55**: 135-159.

606 Zhao Y, Simon M, Seluanov A, et al. 2023. DNA damage and repair in age-related

607 inflammation. *Nature Reviews Immunology*, **23**(2): 75-89.

608 Zhou P, Tachedjian M, Wynne JW, et al. 2016. Contraction of the type I IFN locus and

609 unusual constitutive expression of IFN-alpha in bats. *Proceedings of the National Academy of*

610 *Sciences of the United States of America*, **113**(10): 2696-2701.

611 Zou Y, Zhang M, Zhou J. 2023. Recent trends in STING modulators: Structures, mechanisms,

612 and therapeutic potential. *Drug Discovery Today*, **28**(9): 103694.

613

TABLES and FIGURES

Figure 1. Validation of the successful establishment of bat STING KI mice

A: Schematic of bat STING knock-in mouse generation. Primers (F and R) used for genotype identification were designed. **B**: Representative images of agarose gel electrophoresis for *Md*STING mice genotyping. **C**: Western blot analysis of STING protein to detect exogenous transfected STING plasmids in 293T cells (left) or the endogenous expression of STING in BMDM cells from wild-type mice (n=3) or *Md*STING mice (n=3) (right). **D**: The mRNA expression level of STING gene in different organs of mice (n=4 for each). The primers used for STING gene were mouse- or bat- specific respectively and can be found in Supplementary Table S1. **E**: Splenocytes of wild-type and *Md*STING mice (n =3, cells from 3 animals each) were transfected with cGAMP (2 μg/mL), the induction of *Ifnb* and *Cxcl10* genes was determined by qRT-PCR. Primers can be found in Supplementary Table S1. Data are shown as mean ± s.e.m. *P* values were obtained using two-tails unpaired t-test.

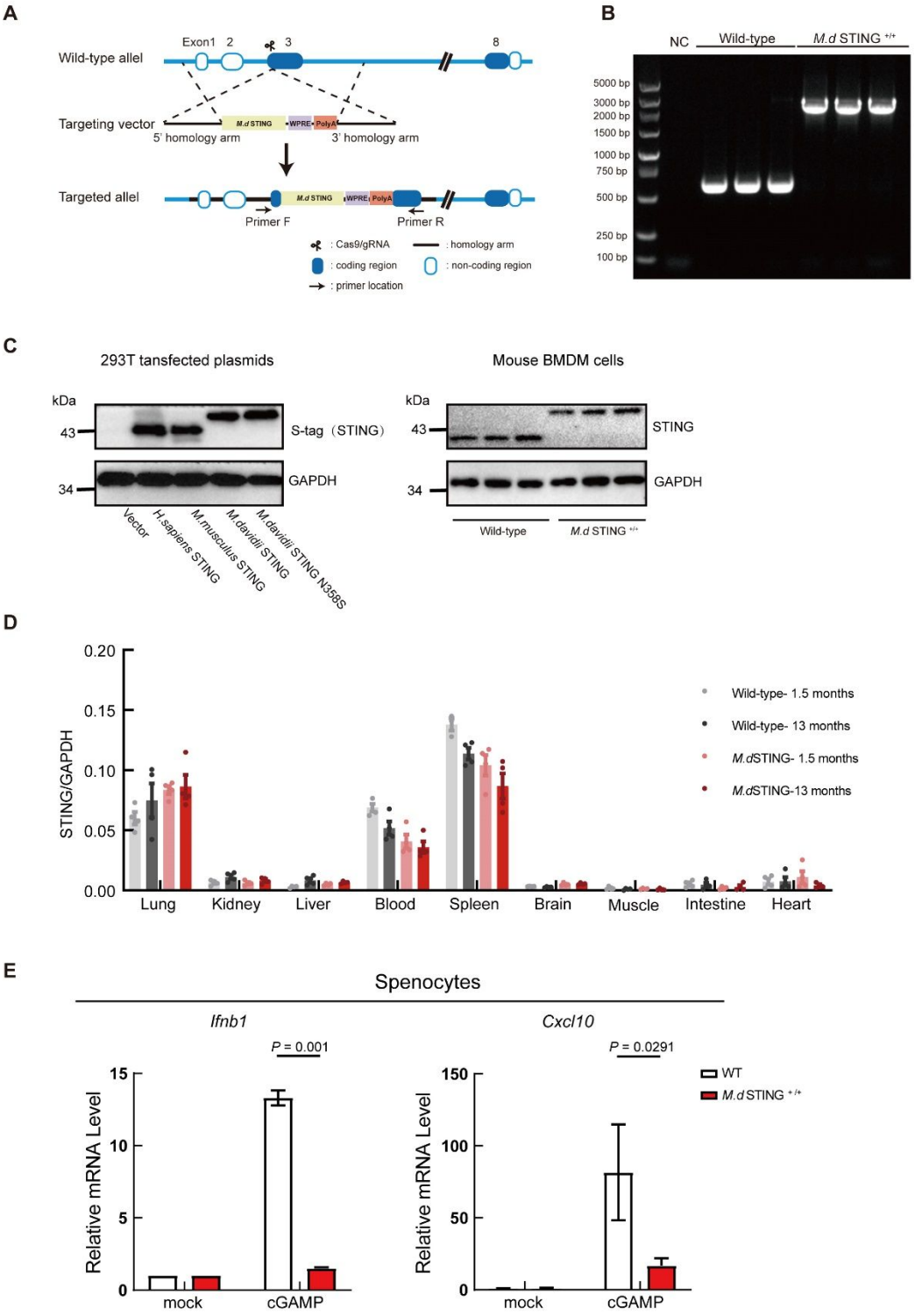
A
Wild-type allel
Exon1 2 3 8
Targeting vector
M.d STING
WPRE
PolyA
5' homology arm
3' homology arm
Targeted allel
Primer F
Primer R
: Cas9/gRNA
: homology arm
: coding region
: non-coding region
: primer location
B
NC
Wild-type
M.d STING +/+
5000 bp
3000 bp
2000 bp
1500 bp
1000 bp
750 bp
500 bp
250 bp
100 bp
C
293T tansfected plasmids
Mouse BMDM cells
kDa
43
34
S-tag（STING）
GAPDH
STING
Vector
H.sapiens STING
M.musculus STING
M.davidii STING
M.davidii STING N358S
Wild-type
M.d STING +/+
D
STING/GAPDH
0.20
0.15
0.10
0.05
0.00
Wild-type- 1.5 months
Wild-type- 13 months
M.dSTING- 1.5 months
M.dSTING-13 months
Lung
Kidney
Liver
Blood
Spleen
Brain
Muscle
Intestine
Heart
E
Spenocytes
Ifnb1
P = 0.001
Cxcl10
P = 0.0291
Relative mRNA Level
15
10
5
0
150
100
50
WT
M.d STING +/+
mock
cGAMP

Figure 1

Figure 2. Longitudinal comparative plasma transcriptomics analysis reveals lower aging-related inflammation in bat STING KI female mice

A: Schematic diagram of longitudinal monitoring and blooding. **B**: GSEA plots showing the trend of significantly changed pathway in aged *Md*STING female mice during aging (upper, downregulated; lower, upregulated). **C**: Number of common or unique pathways in each time point. **D**: Top 5 pathways downregulated at all time points in *Md*STING female mice compared to wild-type female mice. **E**: Top 5 pathways upregulated at all time points in *Md*STING female mice compared to wild-type female mice. **F-G**: The neutrophil (F) or monocyte/macrophage (G) fraction for wild-type female mice or *Md*STING female mice was compared by ImmuCellAI for each time point. Trend of changes were shown on right. The male mice data can be found in Supplementary Figure S4.

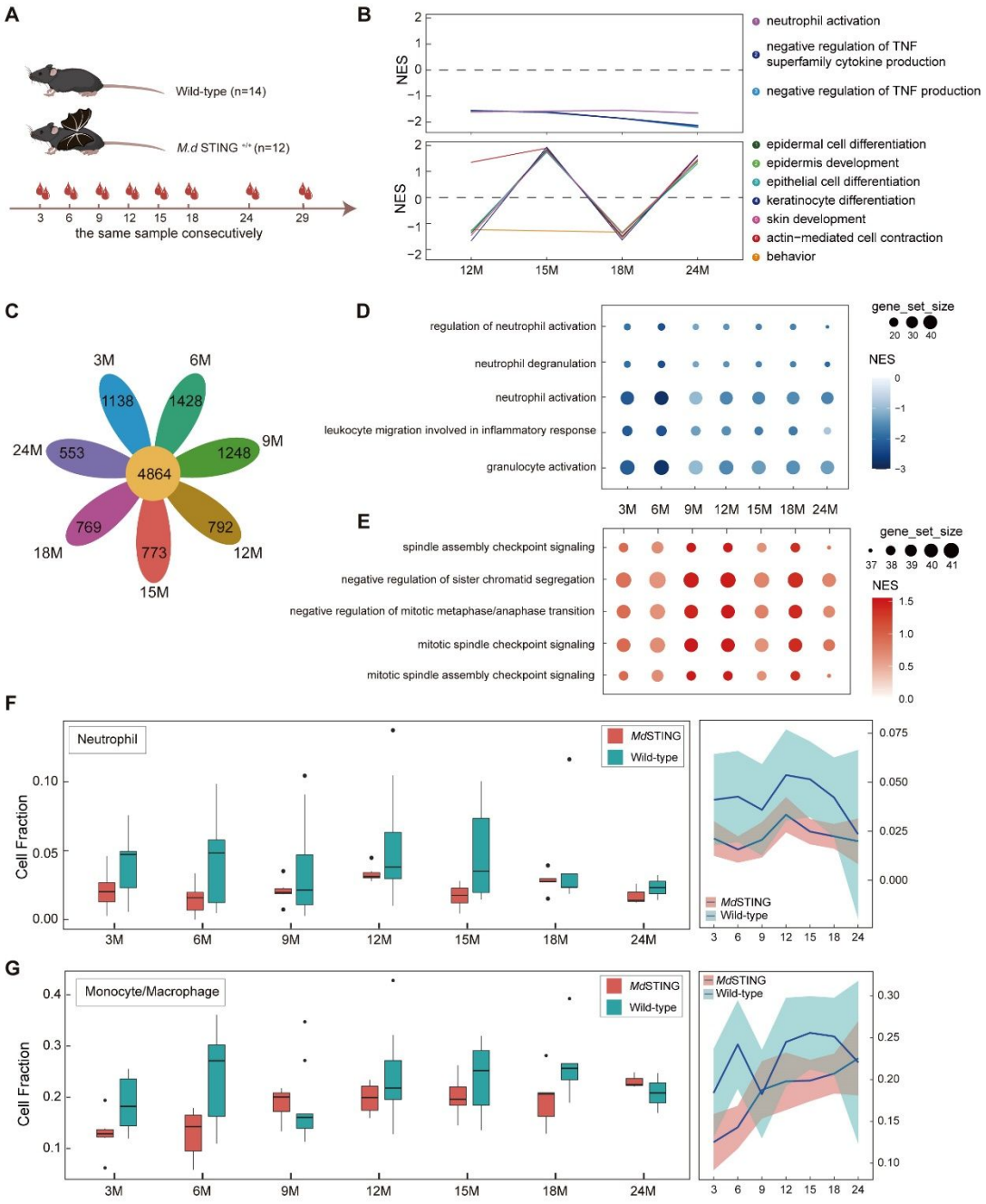
A
Wild-type (n=14)
M.d STING +/+ (n=12)
3 6 9 12 15 18 24 29
the same sample consecutively
B
NES
neutrophil activation
negative regulation of TNF superfamily cytokine production
negative regulation of TNF production
epidermal cell differentiation
epidermis development
epithelial cell differentiation
keratinocyte differentiation
skin development
actin−mediated cell contraction
behavior
12M 15M 18M 24M
C
3M 6M 9M 12M 15M 18M 24M
1138 1428 1248 553 4864 769 792 773
D
regulation of neutrophil activation
neutrophil degranulation
neutrophil activation
leukocyte migration involved in inflammatory response
granulocyte activation
gene_set_size
NES
E
spindle assembly checkpoint signaling
negative regulation of sister chromatid segregation
negative regulation of mitotic metaphase/anaphase transition
mitotic spindle checkpoint signaling
mitotic spindle assembly checkpoint signaling
F
Neutrophil
MdSTING
Wild-type
Cell Fraction
G
Monocyte/Macrophage

Figure 2

Figure 3. *M.d* STING KI reduces pro-inflammatory response in vivo

A: The plasma cytokine expression was detected for either Interleukin-1β (IL-1β) (n=4 for wild-type mice or *Md*STING female mice). **B**: The *Tnf-a* mRNA expression level in aged female mice. **C**: mRNA expression level of pro-inflammatory cytokines in mouse liver, including a panel of cytokines and chemokines. n=4 mice for each group. **D**: mRNA expression level of pro-inflammatory cytokines in mouse kidney, including a panel of cytokines and chemokines. n=4 mice for each group. Data are shown as mean ± s.e.m. *P* values were obtained using two-tails unpaired t-test.

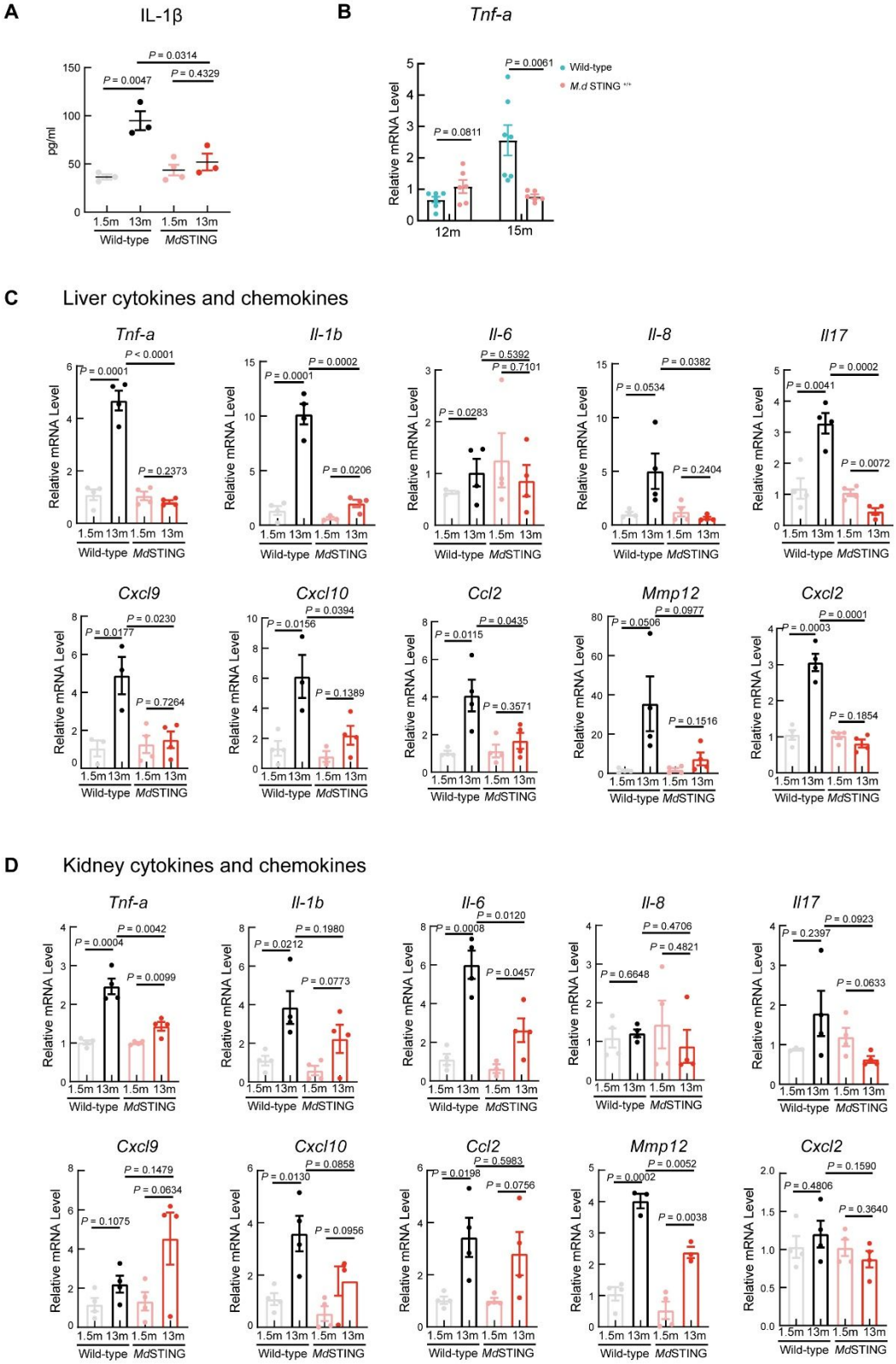
A
IL-1β
pg/ml
P = 0.0314
P = 0.0047
P = 0.4329
1.5m 13m 1.5m 13m
Wild-type MdSTING
B
Tnf-a
Relative mRNA Level
P = 0.0061
P = 0.0811
Wild-type
M.d STING +/+
12m 15m
C
Liver cytokines and chemokines
Tnf-a
P < 0.0001
P = 0.0001
P = 0.2373
Il-1b
P = 0.0002
P = 0.0001
P = 0.0206
Il-6
P = 0.5392
P = 0.7101
P = 0.0283
Il-8
P = 0.0382
P = 0.0534
P = 0.2404
Il17
P = 0.0002
P = 0.0041
P = 0.0072
Cxcl9
P = 0.0230
P = 0.0177
P = 0.7264
Cxcl10
P = 0.0394
P = 0.0156
P = 0.1389
Ccl2
P = 0.0435
P = 0.0115
P = 0.3571
Mmp12
P = 0.0977
P = 0.0506
P = 0.1516
Cxcl2
P = 0.0001
P = 0.0003
P = 0.1854
D
Kidney cytokines and chemokines
Tnf-a
P = 0.0042
P = 0.0004
P = 0.0099
Il-1b
P = 0.1980
P = 0.0212
P = 0.0773
Il-6
P = 0.0120
P = 0.0008
P = 0.0457
Il-8
P = 0.4706
P = 0.4821
P = 0.6648
Il17
P = 0.0923
P = 0.2397
P = 0.0633
Cxcl9
P = 0.1479
P = 0.0634
P = 0.1075
Cxcl10
P = 0.0858
P = 0.0130
P = 0.0956
Ccl2
P = 0.5983
P = 0.0198
P = 0.0756
Mmp12
P = 0.0052
P = 0.0002
P = 0.0038
Cxcl2
P = 0.1590
P = 0.4806
P = 0.3640

Figure 3

Figure 4. Bat STING reduces the aging-related immunopathology

A: The liver tissue from the 1.5 months or 13 months wild-type and *Md*STING female mice were analyzed for immunopathology. HE staining (40×) showing the infiltration of inflammatory cell (black arrow) and Kupffer cells (yellow arrow) for each mice group. Scale bars=20 μm. **B**: A quantification of inflammatory cell infiltration area was performed (n=4 for each). **C**: Immunostaining of Ly6G, representing the infiltration of neutrophils was shown. **D**: A quantification of Ly6G positive cell was analyzed (n=4 for each). **E**: mRNA expression level of *Mpo*, *Cd11b*, *Cxcr2*, *Cxcr4* genes, representing the activation of neutrophils (n=4 for each). Data was shown as mean ± s.e.m. *P* values were obtained using two-tails unpaired t-test.

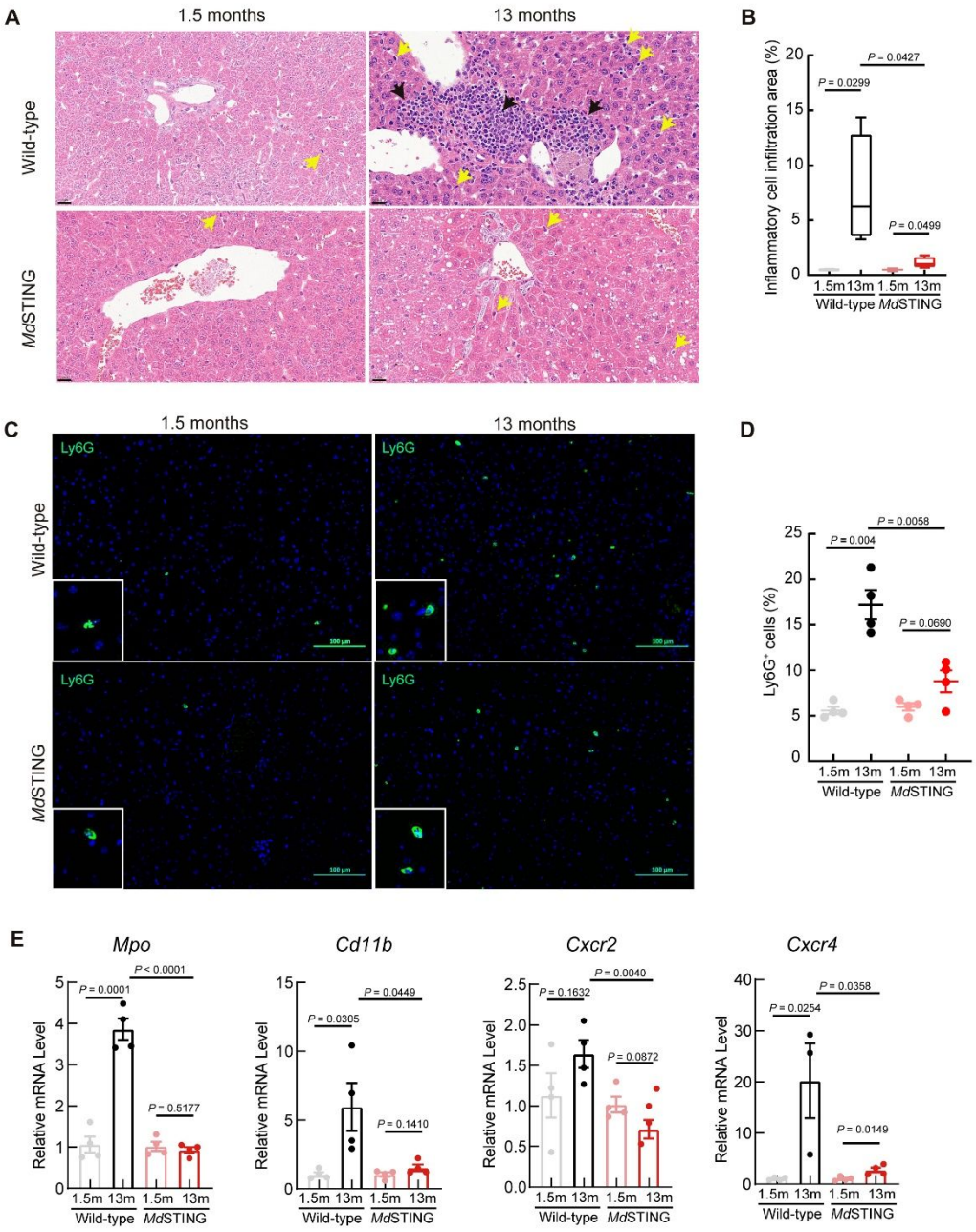

675

676 **Figure 4**

677

678 **SUPPLEMENTARY MATERIALS**

679 **Supplementary Table S1. Primer sequences for qRT-PCR**

Gene name	Forward Primer (5'→3')	Reverse Primer (5'→3')
GAPDH	ACGGCCGCATCTTCTTGTGCA	ACGGCCAAATCCGTTCACACC
STING (WT)	CCGCTCCAAATATGTAGCCCT	CAGTAGTCCAAGTTCGTGCG
STING (*M.d*)	CTTGCACCCATCCATCCCTC	CTGGAGAACGTGTTTTGGCG
TNFα	CCCTCACACTCAGATCATCTTCT	GCTACGACGTGGGCTACAG
IL-1β	ACGGACCCCAAAAGATGAAG	TTCTCCACAGCCACAATGAG
IL-6	AGTTGCCTTCTTGGGACTGA	TCCACGATTTCCCAGAGAAC
IL-8	GTCCTTAACCTAGGCATCTTCG	TCTGTTGCAGTAAATGGTCTCG
CXCL9	CGAGGCACGATCCACTACAA	AGGCAGGTTTGATCTCCGTT
CXCL10	GTGAGAATGAGGGCCATAGG	TTTTTGGCTAAACGCTTTCAT
MMP12	TTCATGAACAGCAACAAGGAA	TTGATGGCAAAGGTGGTACA
CCL2	CCTGCTGCTACTCATTCACCA	ATTCCTTCTTGGGGTCAGCA
MPO	CGTGTCAAGTGGCTGTGCCTAT	AACCAGCGTACAAAGGCACGGT
CD11b	TACTTCGGGCAGTCTCTGAGTG	ATGGTTGCCTCCAGTCTCAGCA
CXCR2	CTCTATTCTGCCAGATGCTGTCC	ACAAGGCTCAGCAGAGTCACCA
CXCR4	GACTGGCATAGTCGGCAATGGA	CAAAGAGGAGGTCAGCCACTGA
CXCL2	CATCCAGAGCTTGAGTGTGACG	GGCTTCAGGGTCAAGGCAAACT
IL-17	CAGACTACCTCAACCGTTCCAC	TCCAGCTTTCCCTCCGCATTGA

680

681

682 **Supplementary Figure S1. Sequencing confirmation of the correct insertion of**

683 **bat STING KI mice and prediction of O-glycosylation sites of the STING protein**

684 **A**: Shown as the N-/C- terminal of the inserted sequence and the strategy used for the

685 contruction of mouse model. The complete sequence of inserted fragment were added

686 to Supplementary data S1. **B**: Prediction of O-(β)-GlcNAc glycosylation and Yin-

687 Yang sites on *Myotis davidii* bat , mouse and human STING proteins, the prediction

688 website is : [https://services.healthtech.dtu.dk/services/YinOYang-1.2/].

689

690

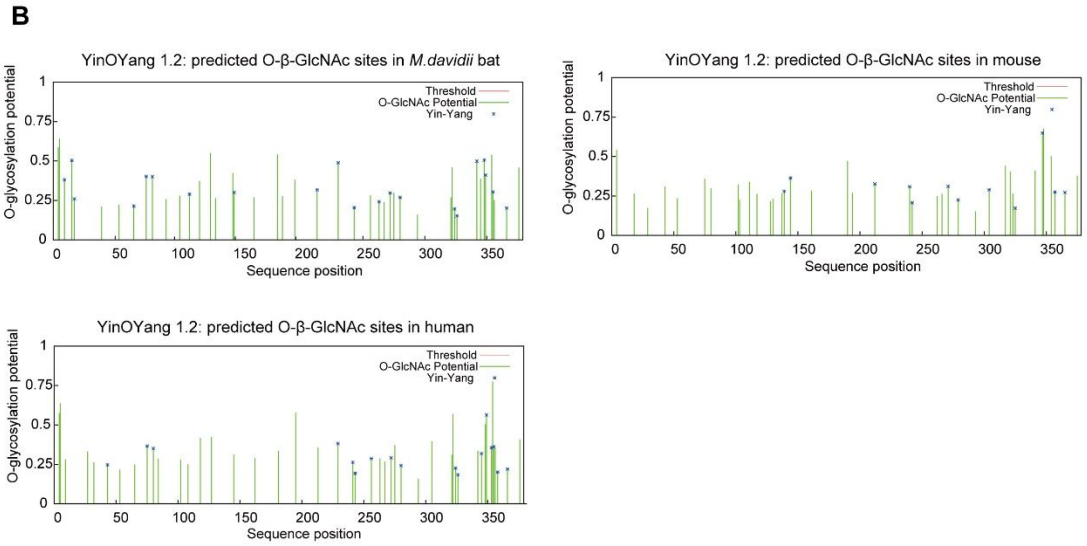

Supplementary Figure S1

Supplementary Figure S2. Weight and survival rates curve (left) and median lifespan(right) for wild-type and *Md*STING mice

A-B: Body weight changes for female (A) or male mice (B). Body weight was not counted after 18-month due to a low cohort number. **C-E**: Survival rates curve (left) and median lifespan (right) for wild-type and *Md*STING of both sex (C), female (D) or male (E) mice. Data are shown as mean ± s.e.m. *P* values were obtained by log-rank test for the survival curves, and two-tails unpaired t-test for lifespan.

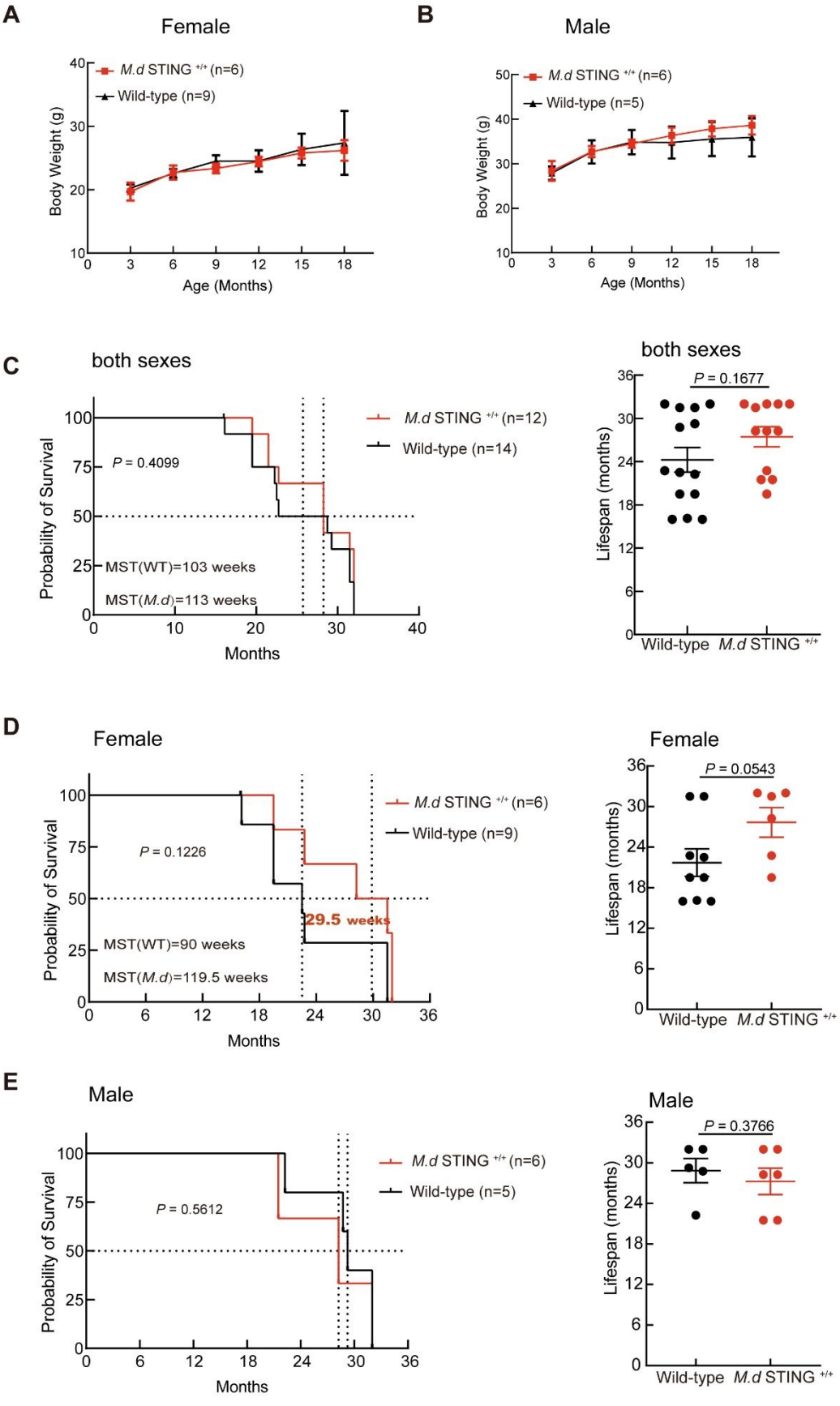

Supplementary Figure S2

Supplementary Figure S3. Attenuated cytokines and inflammatory in the plasma from bat STING KI female mice

The normalized expression of selected cytokines and inflammatory differentially regulated in the blood of wild-type and *Md*STING female mice at 3,6,9,12,15,18 and 24 months, obtained from the RNA-seq data. Data are shown as mean ± s.e.m. *P* values were obtained using unpaired wilcox-test.

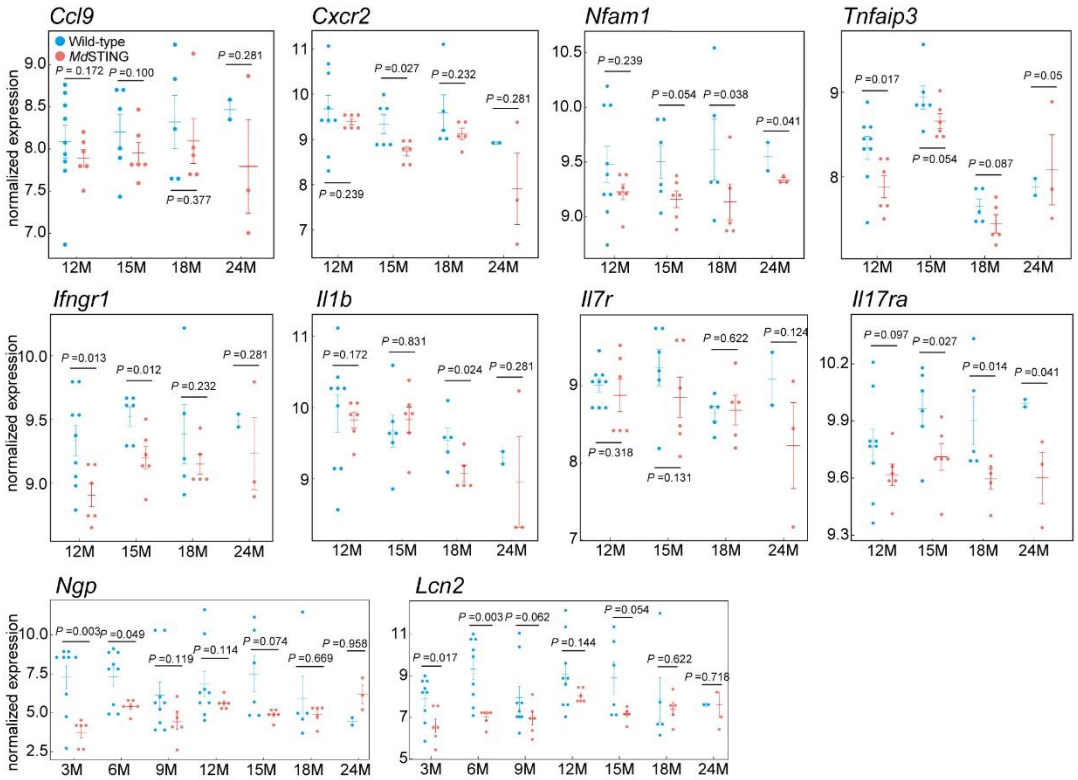

Supplementary Figure S3

Supplementary Figure S4. Longitudinal comparative plasma transcriptomic analysis reveals no significant difference in age-related inflammation between wild-type mice and *Md*STING male mice

A: Normalized expression of selected cytokines and inflammatory differentially regulated in blood of male wild-type and *Md*STING mice at 3,6,9,12,15,18 and 24 months. Data was obtained from RNA-seq and shown as mean ± s.e.m. *P* values shown on the plot were obtained using unpaired wilcox-test and rounded to four decimal places. **B**: Top 5 pathways upregulated (up) / downregulated (down) at all time points in *Md*STING male mice compared to wild-type mice. **C-D**: The monocyte/macrophage (C) or neutrophil (D) fraction for wild-type mice or MdSTING mice was compared by ImmuCellAI for each time point. Trend of changes were shown on right.

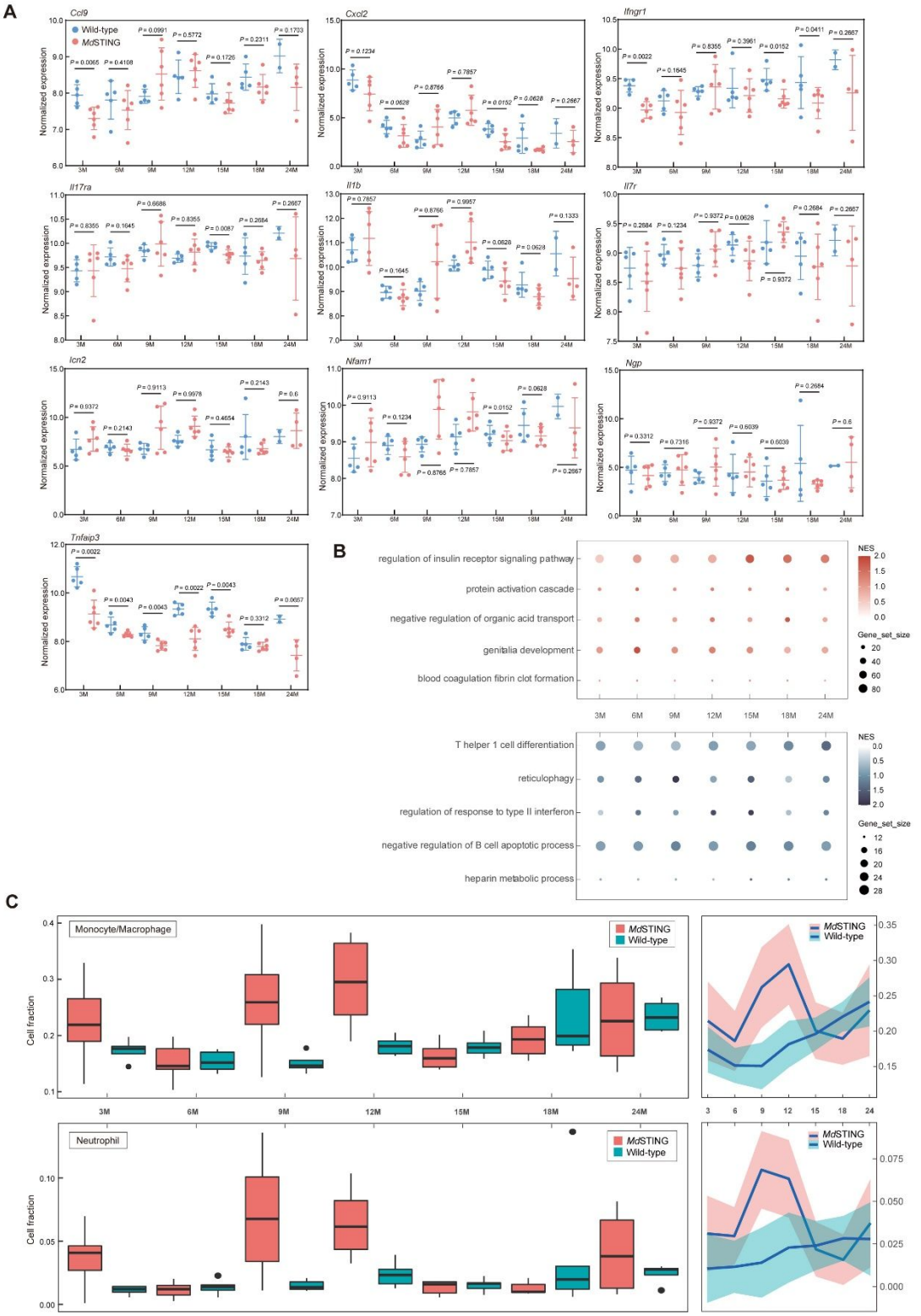

Supplementary Figure S4

Supplementary Figure S5. Pro-inflammatory genes expression pattern in different organs for each mice group

A–F: The mRNA expression level of proinflammatory and chemokines *Tnf-a*, *Il1b*, *Il6*, *Il8*, *Cxcl9*, *Cxcl10* in mouse blood (**A**), lung (**B**), spleen (**C**), heart (**D**), intestine (**E**) and muscle (**F**) (n=4 for each). Data shown as mean ± s.e.m. *P* values were obtained using two-tails unpaired t-test.

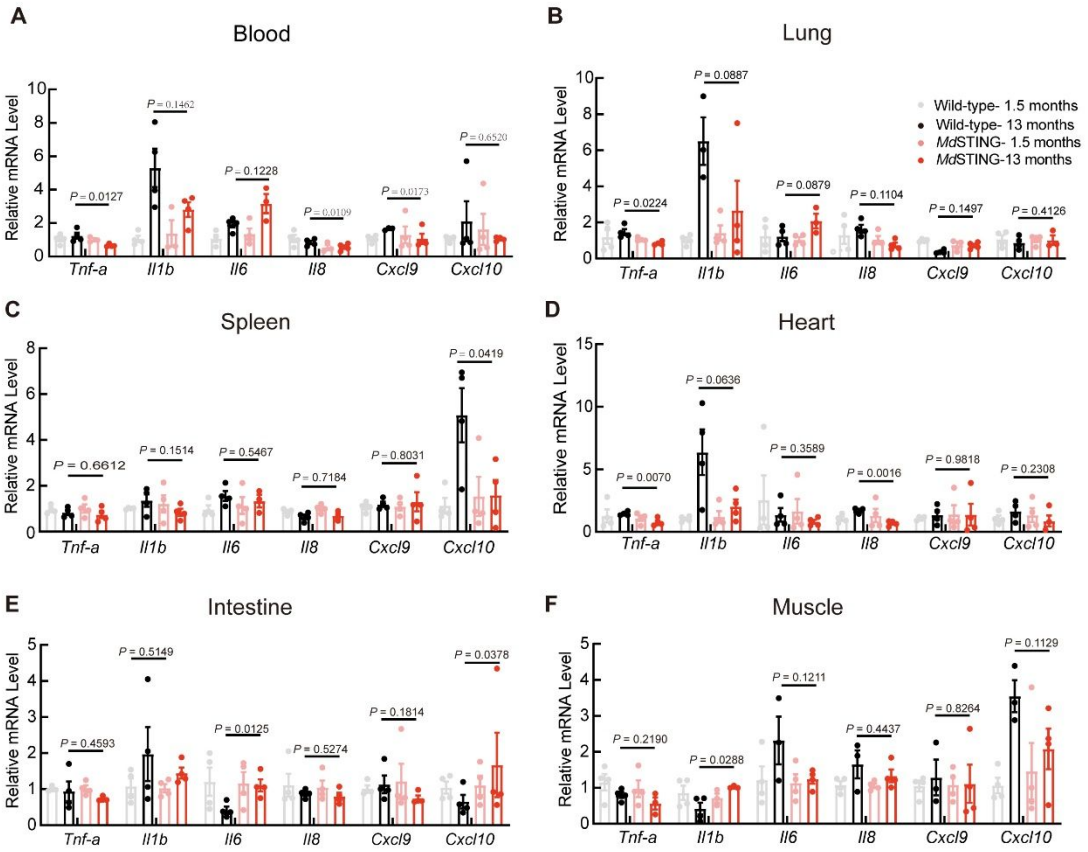

Supplementary Figure S5